REPORT DOCUMENTATION PAGE

Form Approved
OMB No. 0704-0188

1. REPORT DATE *(DD-MM-YYYY)*	2. REPORT TYPE	3. DATES COVERED *(From - To)*
05-02-2010	Journal Article	

4. TITLE AND SUBTITLE

Non-equilibrium Numerical Model of Homogeneous Condensation in Argon and Water Expansions (Preprint)

5a. CONTRACT NUMBER

5b. GRANT NUMBER

5c. PROGRAM ELEMENT NUMBER

6. AUTHOR(S)
Ryan Jansen (USC); Ingrid Wysong (AFRL/RZSA); Sergey Gimelshein, Micheal Zeifman (ERC); Udo Buck (Max-Planck-Institute for Dynamics and Self-Organization, Germany)

5d. PROJECT NUMBER

5f. WORK UNIT NUMBER
23080532

7. PERFORMING ORGANIZATION NAME(S) AND ADDRESS(ES)

Air Force Research Laboratory (AFMC)
AFRL/RZSA
10 E. Saturn Blvd.
Edwards AFB CA 93524-7680

8. PERFORMING ORGANIZATION REPORT NUMBER

AFRL-RZ-ED-JA-2010-036

9. SPONSORING / MONITORING AGENCY NAME(S) AND ADDRESS(ES)

Air Force Research Laboratory (AFMC)
AFRL/RZS
5 Pollux Drive
Edwards AFB CA 93524-7048

10. SPONSOR/MONITOR'S ACRONYM(S)

11. SPONSOR/MONITOR'S NUMBER(S)
AFRL-RZ-ED-JA-2010-036

12. DISTRIBUTION / AVAILABILITY STATEMENT

Approved for public release; distribution unlimited (PA #10052).

13. SUPPLEMENTARY NOTES
For publication in the Journal of Chemical Physics.

14. ABSTRACT

A computational approach capable of modeling homogeneous condensation in non-equilibrium environments is presented. The approach is based on the direct simulation Monte Carlo (DSMC) method, extended as appropriate to include the most important processes of cluster nucleation and evolution at the microscopic level. The approach uses a recombination-reaction energy-dependent mechanism of the DSMC method for the characterization of dimer formation, and the RRK model for the cluster evaporation. Three-step testing and validation of the model is conducted by (i) comparison of clusterization rates in an equilibrium heat bath with theoretical predictions for argon and water vapor and adjustment of the model parameters, (ii) comparison of the non-equilibrium argon cluster size distributions with experimental data, and (iii) comparison of the non-equilibrium water cluster size distributions with experimental measurements. Reasonable agreement was observed for all three parts of the validation.

15. SUBJECT TERMS

16. SECURITY CLASSIFICATION OF:			17. LIMITATION OF ABSTRACT	18. NUMBER OF PAGES	19a. NAME OF RESPONSIBLE PERSON
					Dr. Ingrid Wysong
a. REPORT	b. ABSTRACT	c. THIS PAGE	SAR	14	19b. TELEPHONE NUMBER *(include area code)*
Unclassified	**Unclassified**	**Unclassified**			N/A

Non-equilibrium Numerical Model of Homogeneous Condensation in Argon and Water Vapor Expansions (Preprint)

Ryan Jansen,[1] Ingrid Wysong,[2] Sergey Gimelshein,[3] Michael Zeifman,[4] and Udo Buck[5]
[1)] *University of Southern California, Los Angeles, CA 90089, USA*
[2)] *Air Force Research Laboratory, Edwards AFB, CA 93524, USA*
[3)] *ERC, Inc., Edwards AFB, CA 93524, USA*
[4)] *Luminad Technologies, Boston, MA, USA*
[5)] *Max-Planck-Institut fuer Dynamik und Selbstorganisation, 37073 Goettingen, Germany*

(Dated: 2 February 2010)

A computational approach capable of modeling homogeneous condensation in non-equilibrium environments is presented. The approach is based on the direct simulation Monte Carlo (DSMC) method, extended as appropriate to include the most important processes of cluster nucleation and evolution at the microscopic level. The approach uses a recombination-reaction energy-dependent mechanism of the DSMC method for the characterization of dimer formation, and the RRK model for the cluster evaporation. Three-step testing and validation of the model is conducted by (i) comparison of clusterization rates in an equilibrium heat bath with theoretical predictions for argon and water vapor and adjustment of the model parameters, (ii) comparison of the non-equilibrium argon cluster size distributions with experimental data, and (iii) comparison of the non-equilibrium water cluster size distributions with experimental measurements. Reasonable agreement was observed for all three parts of the validation.

I. INTRODUCTION

The phenomenon of homogeneous condensation has regained significant interest recently, partly because it is directly related to the nanofabrication[1,2] and partly because of the advances in the experimental[3] and theoretical[4] methods. Unlike other first-order phase transitions, the gas-to-liquid transition often occurs in a non-equilibrium environment, e.g., in a rapid gas expansion. The transient events, characteristic of the condensation in a non-equilibrium environment, are still difficult for direct experimental observation, making validation of both empirical correlations and theoretical predictions challenging. A computational method capable of reproducing diverse experimental condensation scenarios, including both equilibrium and non-equilibrium condensations, can provide a viable alternative to these methods.

Two different approaches for modeling the condensation in such non-equilibrium environment as rapidly expanding plumes have been reported in the literature. The first approach, known as the classical approach, takes its starting point from the classical nucleation theory (CNT) which is based on equilibrium thermodynamics.[5,6] The second one, known as the kinetic approach, treats nucleation as the process of kinetic chemical aggregation.[7]

The classical approach considers the energy of cluster formation from the vapor state. Assuming unimolecular reactions of cluster growth and decay, CNT calculates the corresponding condensation and evaporation rates using the Gibbs distributions and the principle of detailed balance[7–10]. The nucleation rate is then calculated assuming a steady state condition.[11] Although a rapidly expanding supersonic plume is quite different from the isothermal, ideal gas environment assumed by CNT, the classical predictions were found to be qualitatively correct for the modeling of cluster formation in supersonic jets.[12–16] There are many examples, however, when CNT-based results cannot be fitted to experimental data. The CNT-based prediction of the cluster size distributions[17] significantly deviated from experimental data.[18] This is consistent with the work of Ref. 19, where it was also found that the correct prediction of the cluster size distribution along with the internal and translational energy distributions is beyond the area of applicability of the classical approach.

The reasons for the discrepancy between the CNT-based distributions and experimental data are both due to problems inherent in CNT and the flow conditions of expanding plumes. The former include the ambiguous definition of the surface energy of small clusters,[11] the neglect of the rotational and translational degrees of freedom of freshly nucleated clusters,[20] and the unrealistic description of vapor-cluster and cluster-cluster interactions.[16] The latter are related to the main assumptions underlying the derivation of the nucleation rate, which may be violated in rapidly expanding supersonic flows.[21] The transient time needed for a system to reach steady state in terms of the unimolecular cluster reactions may be such that the jet macroparameters will significantly change during that time. Moreover, many theoretical and experimental results[22–24] suggest that local thermal equilibrium does not exist in an expanding supersonic jet. Thus the process of cluster formation is not likely to be isothermal. There have been recent advances in CNT mainly aimed at achieving a more realistic model for condensation and evaporation rates,[10,20,25–28] but other principal deficiencies of CNT and its application to the non-equilibrium environment still have yet to be addressed. Note that despite these deficiencies, the steady state CNT nucleation rate with a correction[10] is

used in such commercial fluid dynamics codes as GASP or CFD-particle.

Unlike CNT, the kinetic approach does not assume local thermodynamic equilibrium. Instead, a microscopic view of the interactions of monomers and clusters is established either analytically via a mathematical model, e.g., by the Smoluchowski equations where the interaction between particles is modeled by the reaction rates,[9,29,30] or in computer simulations, e.g., in molecular dynamics (MD) calculations where the interaction is modeled by an interaction potential.[31–33] It can be shown that the application of the Smoluchowski equations to the modeling of clustering in supersonic jets is computationally unfeasible. Even though MD simulations might seem attractive (since no information besides the interaction potential is needed to perform the calculations), they are computationally limited to a system size of about one million gas particles and a time scale of a few nanoseconds at most. In real plumes, such as thruster nozzles or ablation jets, the number of gas particles and the expansion time is greater by many orders of magnitude (see, for example,[13,34]). Therefore, the MD technique cannot be directly applied to the simulation of even small laboratory-sized supersonic jets.

A promising direction in modeling the coupled condensation flow is the use of a kinetic particle simulation method, direct simulation Monte Carlo (DSMC),[35] which is applicable in a wide range of flow regimes from free molecular to near continuum. It is a statistical approach for solving the spatially nonuniform master Leontovich equation for the N-particle distribution function and, in the limit of a large N, it represents an accurate solution of the Boltzmann equation. The advantage of DSMC as compared to other methods is that complicated cluster-cluster and cluster-monomer interactions including the multi-body reactions of cluster nucleation can be seamlessly incorporated.

The DSMC method has been used to study the process of cluster formation and evolution for a number of years.[9,36,37] However, the gas flow in the earlier studies was uniform, the considered cluster size range was very narrow (up to 25 monomers in a cluster) and the examined reaction types were unrealistically limited to elastic collisions, cluster and monomer sticking to clusters, and evaporation of monomers from clusters.

More recently, the DSMC method has been extensively and successfully applied to modeling the processes of cluster formation and evolution in supersonic jets by Levin et al (see, for example, Refs. 16,38,39). The model initially was based on the classical nucleation theory, with the new clusters being formed at the critical size. Further work of these authors[40] extended the kinetic dimer formation approach of Ref. 41, who assumed that a ternary collision always results in a dimer formation, to include molecular dynamic (MD) simulations for obtaining information on the probability of dimer formation in such ternary collisions The work[42] used a temperature-dependent probability of formation of argon dimers.

Although the use of MD has a number of advantages, due to its inherent limitations, the obtained probability cannot be unambiguously related to such characteristics of the ternary collision as the internal energy of the collision complex and the kinetic energy of the impinging monomer. Another possible limitation of the above work is that the cell quantities (e.g., temperature) rather than individual particle characteristics are used in the microscopic models of nucleation and evaporation.

In the present paper, the DSMC approach for modeling of homogeneous nucleation in rapidly expanding plumes is extended to include a number of new features. Firstly, all microscopic reactions are modeled using the characteristics of individual particles and not those averaged over DSMC cells. Secondly, a truly kinetic RRK model[44] is implemented to characterize the cluster evaporation rates. Then, an energy dependent collision procedure similar to the recombination reaction model of Ref. 45 is used for the collision complex formation. An empirical parameter is used for the inelastic collision number in the cluster-monomer collisions. For dimers, this parameter was calibrated through the comparison of the computed nucleation rates and equilibrium constants in thermal bath with available theoretical and experimental data for argon and water. Additional validation analysis is conducted through direct comparison with reliable measurements of cluster size distributions in argon[47] and water[48].

II. COMPUTATIONAL MODEL OF HOMOGENEOUS NUCLEATION

In the present non-equilibrium model of homogeneous condensation formulated for the DSMC method, all of the most important processes of cluster nucleation and evolution are considered at the microscopic level. First principles of the kinetic theory are used to define the main processes of homogeneous condensation, where all collision, nucleation, and evaporation events depend on instantaneous energies of colliding partners, and not cell temperature or other macroscopic quantities. The processes that are included in the model and described in detail below are (i) formation of collision complexes through the binary collisions of cluster-forming monomer species, (ii) creation of dimers through the collision stabilization of collision complexes, (iii) elastic monomer-cluster collisions that change the translational and internal energies of colliding particles, (iv) inelastic monomer-cluster collisions that result in monomer sticking, (v) cluster-cluster coalescence, (vi) evaporation of monomers from clusters. The details on each of these processes are given below.

A. Collision complex formation

One of the important assumptions of the present model is that all pairs of colliding particles create collision com-

plexes. A collision complex is a pair of monomers that have collided, and may have the conditions necessary to form a dimer if struck by a third particle during its lifetime. The collision complex lifetime, t_l, is assumed to be dependent on the type of monomers and their relative collision velocity, with the functional dependence given by the well known Bunker's expression[49]

$$t_l = 1.5\sigma_0\mu^{\frac{1}{2}}\epsilon_0^{\frac{1}{6}}E^{-\frac{2}{3}}, \tag{1}$$

where σ_0 and ϵ_0 are the potential depth and separation distance parameters of the Lennard-Jones (LJ) potential, μ is the reduced mass of the colliding particles, and E is their relative translational energy. The values of σ_0 and ϵ_0 used in this work are 3.2×10^{-10} m and 7.94×10^{-21} J for water, and 3.405×10^{-10} m and 1.654×10^{-21} J for argon. The argon LJ parameters are well known, but H_2O values are roughly estimated by reproducing the known viscosity of water vapor at 273 K and for a small range of temperatures using a LJ potential model.

The process of interaction of collision complexes with surrounding gas particles is modeled using the majorant frequency scheme[50] with the assumption that the collision complex - third particle interactions are governed by the Variable Hard Sphere (VHS) interaction model.[51] The VHS viscosity-temperature exponent ω of a collision complex was assumed to be that of the comprising monomers. For argon atoms, the VHS parameters taken from Ref. 35 were assumed, $d_{ref} = 4.17$ Å and $\omega = 0.81$. For water molecules, $d_{ref} = 6.2$ Å and $\omega = 1$ were assumed, based on reproducing the known viscosity of water vapor at 273 K and for a small range of temperatures using the VHS potential model. Note that the VHS collision diameters are used to compute collision frequency in the cell, while the LJ diameters are only used for computing the diameter and lifetime of a collision complex in order to determine the probability of a three-body collision.

Generally, the probability $P(\tau)$ that a collision complex will collide with a third particle during an arbitrary time τ is

$$\frac{dP(\tau)}{d\tau} = \nu(1 - P(\tau)) \tag{2}$$

where ν is the collision frequency of the collision complex with third particles. For a mixture of N_s gas species, ν is expressed as

$$\nu = \sum_{i=1}^{N_s} n_i\langle\sigma g\rangle, \tag{3}$$

where σ is the corresponding total collision cross-section, g is the relative collision velocity between particles, and brackets denote averaging over g. Obviously, the probability that the collision complex will move freely and not collide during τ is given by

$$P_{free}(\tau) = e^{(-\tau\nu)}. \tag{4}$$

This expression represents the probability that no dimer will be formed during τ. Using the inverse transform,

$$\tau_c = -\ln(R)/\nu, \tag{5}$$

where R is a random number uniformly distributed between 0 and 1. The majorant frequency algorithm for each pair of colliding monomers is therefore as follows.
1. Calculate t_l and $\nu_{majorant}$ and set $t_0 = 0$, $i = 1$. Here, $\nu_{majorant} = n\overline{\sigma_{max}g_{max}}$ is the majorant collision frequency, and σ_{max} and g_{max} are maximum cross section and relative collision velocity, respectively.
2. Calculate

$$t_i = t_{i-1} - \frac{\ln(R)}{\nu_{majorant}} \tag{6}$$

3. If $t_i > t_l$, go to the the next pair of monomers.
4. If $t_i < t_l$, then a physical collision occurs with a probability $P_c = \frac{\nu(g)}{\sigma g}\sigma_{max}g_{max}$. With a probability $1 - P_c$, $i = i + 1$ and the algorithm returns to step 2.

In this algorithm, for consistency with the collision complex lifetime determination, an expression for the diameter d of the collision complex recommended in Ref. 49 was used,

$$d = 3^{\frac{1}{2}}\sigma_0(\epsilon_0/E)^{\frac{1}{6}}. \tag{7}$$

B. Dimer stabilization

If there is a physical collision between a collision complex and a third particle, there is a possibility of forming a stable dimer as a result of such a collision. Generally, the probability of the formation of a stable dimer (dimer stabilization) depends on the colliding species and the energies - both translational and internal - of the colliding particles. In this work, constant stabilization probabilities of 0.25 for Ar^{40} and 0.7 for H_2O were assumed, which seem reasonable for the range of temperatures under consideration.

Dimer creation through the collisional stabilization of collision complexes is modeled as a two-step process, $L + M \rightarrow (LM)$, $(LM) + K \rightarrow LM + K$. Here, L and M are monomers, (LM) is the collision complex, and K is the third particle. The algorithm of this process is described below.
1. Velocities of the collision complex are calculated from the momentum conservation as

$$\bar{v}_{(LM)} = \frac{m_L\bar{v}_L + m_M\bar{v}_M}{m_{(LM)}} \tag{8}$$

2. The internal energy of the collision complex is calculated from energy conservation,

$$E^{int}_{(LM)} = E^{int}_L + E^{int}_M + \Delta E, \tag{9}$$

where $\Delta E = 0.5(m_{(LM)}v^2_{(LM)} - m_Kv^2_L - m_Lv^2_M)$.

3. The total energy of the collision complex – third particle pair is increased by the evaporation (or binding) energy E_{evap},

$$E^{total} = E^{rel}_{(LM)-K} + E^{int}_{(LM)} + E^{int}_{K} + E_{evap}. \quad (10)$$

Here, $E^{rel}_{(LM)-K}$ is the relative translation energy of the $(LM) - K$ collision. Evaporation energy is a function of cluster size, and the values used for Ar and H_2O are given in the following sections. Note that E^{rot}_K may be used instead of E^{int}_K, since the vibrational mode of third particles will barely be excited at the low temperatures at which homogeneous condensation usually occurs.
4. New energies $E^{rel}_{(LM)-K}$, $E^{int}_{(LM)}$, E^{int}_K are sampled using the Larsen-Borgnakke scheme[52] extended to multiple energy modes.[35]

C. Elastic and inelastic reflective collisions of monomers and clusters

The collisions between monomers and clusters are one of the key processes that determine the nucleation rate. The reason for this is the strong dependence of the evaporation rate on the cluster internal energy. Since the monomers are dominant in the flows considered here, the cluster internal energy is mostly governed by its relaxation through cluster-monomer collisions. In this work, a hard sphere model is assumed for cluster-monomer collisions, with the cluster diameter determined from Eqn. 7 for dimers, and for larger clusters from an empirical correlation used extensively in the past (see, for example, Ref. 16),

$$d = 2 \cdot (A \cdot i^{\frac{1}{3}} + B), \quad (11)$$

where A and B are species-dependent constants, and i is the number of monomers in the cluster. In this work, the values of A and B were 2.3×10^{-10} m and 3.4×10^{-10} m for argon,[38] and 1.9×10^{-10} m and 2.4×10^{-10} m for water.[53]

For the energy transfer between the relative translational and internal modes of the cluster and monomer, the Larsen-Borgnakke model[52] is used, and a parameter Z is introduced which has a meaning of the internal energy relaxation number. The energy transfer between all energy modes of the cluster-monomer pair occurs with a probability Z^{-1}, and an elastic collision with no internal energy exchange occurs with the additional probability $1 - Z^{-1}$. For argon, temperature dependent values of $Z(T)$ were used, obtained through the linear interpolation between the values given in Table I. Similar to temperature dependent collision numbers for rotational and vibrational relaxation of molecules widely used in the DSMC method, T was the cell-based translational temperature. Such a temperature dependence allows good agreement of the DSMC rates for dimer nucleation and dissociation with rates available in the literature. For water condensation, a constant value of $Z = 10$ was used, which corresponds to that for rotational and vibrational relaxation of water molecules at room temperature obtained in molecular dynamics studies.[54,55] For argon, the values of Z given in Table I are used, based on the fitting described in Section III.

TABLE I. Inelastic collision number as function of temperature for argon.

T, K	0.0	100.0	200.0	300.0	400.0	500.0
Z^{-1}	0.25	0.13	0.08	0.06	0.046	0.04

TABLE II. Sticking probability as function of cluster size for argon.

Cluster size	Probability
2	0.06
3	0.075
4	0.1
5	0.16
6	0.3
7	0.5
8	0.67
9	0.75
10	0.8
11	0.833
12	0.857
13	0.876
14	0.891
15	0.9

D. Sticking collisions of monomers and clusters

When a monomer collides with a cluster, sticking of the monomer to the cluster surface is possible, in addition to a reflective collision described in the previous section. For small clusters, monomer sticking is the main process that governs the evolution of the droplet size distribution.[48] For water molecules, an empirical dependence of the sticking probability on the species radius and mass, given in Ref. 56, is used. This dependence reduces to

$$\epsilon = \frac{d_n^2}{(d_n + d_1)^2} \left(\frac{m_n}{m_n + m_1} \right)^{\frac{1}{2}}, \quad (12)$$

where indices n and 1 refer to the cluster and monomer, respectively. Note that for low n this expression agrees well with the molecular dynamics results of Ref. 57. For argon, the sticking probability of monomers on clusters given in Table II is used, based on the results of molecular dynamics simulations of Ref. 38.

The following algorithm is used to model sticking of a molecule to a cluster L to form a larger cluster K.
1. Calculate velocities of K as

$$\bar{v}_k = \frac{m_L \bar{v}_L + m_M \bar{v}_M}{m_k} \quad (13)$$

2. After velocities $\bar{v}_K$ are assigned, the new internal energy is calculated

$$E_K^{int} = E_L^{int} + E_M^{int} + Q + \Delta E \tag{14}$$

Here,

$$\Delta E = -0.5(m_K \bar{v}_K^2 + m_L \bar{v}_L^2 + m_M \bar{v}_M^2)$$

and $Q \equiv E_{evap}$ is the evaporation energy of one monomer off cluster K.

Similar to monomer-cluster collisions, the outcome for cluster-cluster collisions is assumed to be either coalescence or elastic interaction. The probability of sticking was assumed to be unity both for argon and water in cluster-cluster collisions. The algorithm for cluster-cluster sticking collisions is similar to the monomer-cluster collision, with the exception of $Q = -Q_K + Q_L + Q_M$, where Q_i is the energy of vaporization of cluster i.

E. Evaporation rate and algorithm

Following Ref. 34, RRK theory is used to model the evaporation process. The evaporation rate k_e is calculated as

$$k_e = \nu N_s \left(\frac{E_{int} - E_{evap}}{E_{int}} \right)^{3n-7} \tag{15}$$

Here, n is the number of monomers in the cluster, ν is the vibration frequency, N_s is the number of surface atoms, E_{evap} is the evaporation energy, and E_{int} is the cluster internal energy. For dimers, the exponent $3n-7$ is replaced with 1. The number of surface atoms N_s is n for $n < 5$, $n-1$ for $4 < n < 7$, and $(36\pi)^{1/3}(n^{1/3}-1)^2$ for $n > 6$. The vibration frequency was taken to be 2.68×10^{12} s^{-1} for water clusters,[58] and 10^{12} s^{-1} for argon clusters.[58]

Since

$$\frac{dN_s}{dt} = -k_e N_s, \tag{16}$$

the time τ to the next evaporation event for a given cluster may be sampled from $\tau = -\ln \frac{R}{k_e}$. The algorithm used to model the evaporation process for a given cluster over a simulation timestep Δt is as follows.

1. Set $t_{local} = 0$
2. Calculate k_e
3. Change $t_{local} = t_{local-1} - ln(R)/k_e$
4. If $t_{local} > \Delta t$, exit.
5. Evaporate one monomer (see below).
6. If the remaining cluster is a monomer, exit. Else, go to Step 3.

Note that in a limiting case of large clusters (cluster size tends to infinity), Eqn. (15) reduces to an exponential expression similar to that recently obtained using the unimolecular evaporation theory.[59]

F. Energy redistribution in evaporation

The following energy redistribution scheme is used to model the evaporation of a monomer M off a cluster K, with a daughter cluster L formed.

1. Decrease the internal energy of K by the evaporation energy E_{evap}

$$E_K^{int} = E_K^{int} - E_{evap} \tag{17}$$

2. Split cluster internal energy E_K^{int} between the relative translational energy E_{rel} and the internal energy of the M – L pair (the sum of the daughter cluster internal energy and the monomer internal energy), E_{int} using the Larsen-Borgnakke procedure.
3. Split energy E_{int} between the daughter cluster internal energy and the monomer internal energy using the Larsen-Borgnakke procedure.
4. Calculate new daughter cluster and monomer velocities using E_{rel}, keeping in mind that the center of mass of the new pair has the same velocity as the velocity of the original cluster.

G. Evaporation energy and the number of internal degrees of freedom

It is important to use reasonable values for the evaporation energy of a monomer off a cluster, as well as the number of cluster internal degrees of freedom, as a function of cluster size. The reason for this is that all energy redistribution processes that involve clusters depend directly on the number of internal degrees of freedom. The evaporation energy of a monomer from an n-cluster is given by $E_b(n) - E_b(n-1)$, where E_b is the binding (energy to separate all n monomers in an n-cluster) energy of the n-cluster. The E_b values for water clusters (Ref. 60) were taken from Ref. 61 for $n = 2-8$ (and subtracting the zero-point energies, taken from Ref. 62), and using smoothed values from Refs. 63,64 for $n = 9-13$. Evaporation energies were taken from Ref. 65 for argon clusters. The number of cluster internal degrees of freedom is calculated from the expression for the average internal energy $\langle E \rangle$ of a cluster of a size n

$$\langle E \rangle = \frac{\xi^{int}}{2} kT = nC_v T - \frac{3}{2} kT$$

as

$$\xi^{int} = n\frac{2C_v}{k} - 3$$

where C_v is the cluster heat capacity. For water, the values of C_v where adapted from Refs. 66,67. For water dimers, the value of C_v was taken from Ref. 67 at 200 K, and the number of degrees of freedom was assumed to be a function of internal energy (or effective temperature), decreasing linearly from its listed value at 200 K to 3 at 0 K. The heat capacity for $n = 8$ and $n = 10$ was taken

TABLE III. The water and argon cluster heat capacities and evaporation energies per monomer.

Size	H_2O E_{evap}, J	H_2O C_v, J/K	Ar E_{evap}, J	Ar C_v, J/K
2	2.455E-20	3.726E-23	1.98E-21	2.41E-23
3	5.352E-20	4.830E-23	3.96E-21	2.76E-23
4	6.325E-20	5.748E-23	5.94E-21	3.10E-23
5	4.726E-20	6.555E-23	6.08E-21	3.31E-23
6	4.587E-20	7.245E-23	6.89E-21	3.44E-23
7	5.560E-20	7.817E-23	7.49E-21	3.54E-23
8	6.950E-20	8.277E-23	6.36E-21	3.62E-23
9	5.560E-20	8.648E-23	8.29E-21	3.68E-23
10	5.699E-20	8.970E-23	8.25E-21	3.72E-23
11	5.838E-20	9.227E-23	8.27E-21	3.76E-23
12	5.977E-20	9.467E-23	9.86E-21	3.79E-23
13	6.116E-20	9.654E-23	12.2E-21	3.82E-23

from Ref. 66 at 200 K. The values of C_v were interpolated between $n = 2$, 8, 10, and the bulk liquid value. For argon, the values of C_v were assumed to approximate an expression $\xi^{int} = 2(3n - \eta) + \epsilon$, where $\eta = 5$ and $\epsilon = 2$ for $n = 2$ and $\eta = 6$ and $\epsilon = 3$ otherwise.[68] Both the heat capacity and evaporation energies are listed in Table III. For the cluster sizes larger than given below, the values for the maximum listed sizes are used.

The non-equilibrium condensation model described here was implemented in the DSMC code SMILE[69]. The validation of the code through the comparison with theoretical and experimental results is presented below.

III. THERMAL BATH RELAXATION

Inelastic cross sections for monomer-monomer and monomer-cluster collision processes are necessary for detailed validation of a kinetic condensation model. These cross sections, generally functions of the energy states, both translational and internal, of pre- and post-collisional particles, are not available for most gas and temperature conditions of interest. Contrary to the energy dependent cross section, the integral temperature dependent rates for such collisions at conditions close to equilibrium are available in the literature for argon dimers. Therefore, one of the key indicators of the accuracy and reliability of a condensation model is its ability to produce realistic rates of evaporation and nucleation at equilibrium. Although matching the rates generally does not guarantee correct behavior in nonequilibrium, it still is a necessary condition for a model to satisfy.

In this work, thermal bath relaxation of pure argon and pure water vapor are examined at different temperature conditions with the DSMC method, and the dimer formation rates for argon and equilibrium constants for the formation of dimers in argon and water are calculated and compared to the published results.[67,70–73] In all thermal bath results, one million simulated particles were used, and the run proceeded until the steady state is reached, after which the results were sampled for 20 thousand

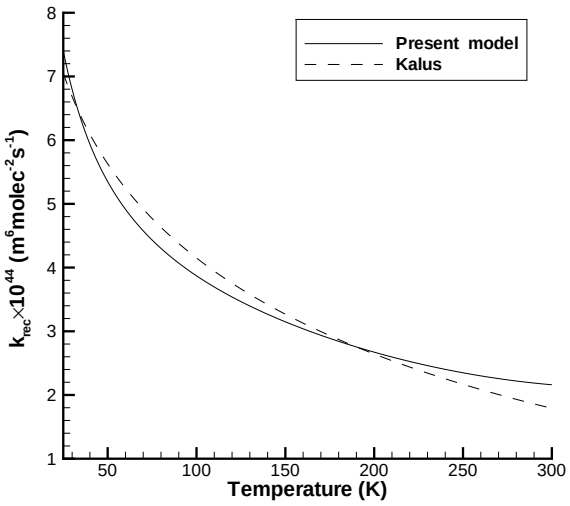

FIG. 1. Argon dimer formation rate as a function of gas temperature.

timesteps. The number density was 5×10^{23} molec/m^3 for argon and 2×10^{23} molec/m^3 for water. The timestep of 2.5×10^{-11} s was selected so that the number of collisions per molecule is much smaller than unity, and the results are independent on the timestep.

The computed dimer formation rates k_{rec} for argon are presented in Fig. 1 and compared with the stable dimer formation rate of Ref. 70, where they were calculated using classical trajectories, and the following expression was proposed,

$$k_{rec} = 10.15T^{-0.278} \exp\{-0.0031T\}. \qquad (18)$$

Generally, the present dimer formation rates are in good agreement with the classical trajectory calculations, with the maximum difference approaching 20% for higher temperatures. Note that the computed rate has a somewhat different slope than that of Eqn. 18. A number of factors could be affecting the slope, among which are the energy dependence of the stabilization probability and dimer heat capacity, which were not included in the present model. The MD calculations in Ref. 40 for argon dimer formation predicted a small decrease in stabilization probability with increasing temperature over a limited temperature range.

The computed equilibrium constant, K_{eq}, which is the ratio of the dimer dissociation to the dimer formation rate, is given in Fig. 2. It is compared to the theoretical results of Ref. 71, where a number of approximate classical and quantum methods are compared with exact numerical calculations, and also experimental results of Ref. 72 and theoretical results of Ref. 73. Note that while the results for different models and interaction potentials were found to be widely different in Ref. 71, there was a good agreement between analogous quantum and classi-

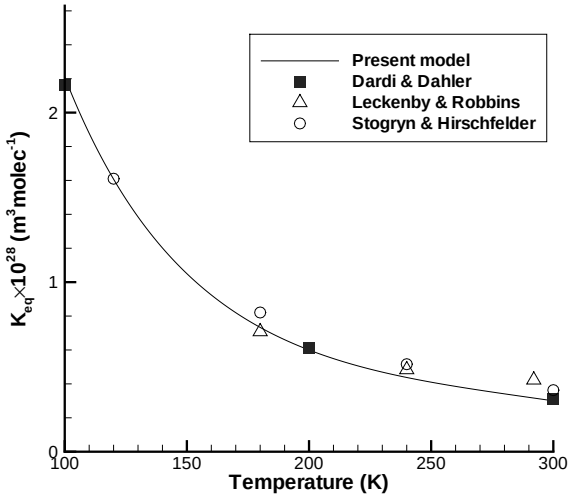

FIG. 2. Argon dimer formation equilibrium constant as a function of gas temperature.

cal calculations. Figure 2 shows that for the entire temperature range there is an excellent agreement between the present model and the theoretical and experimental values. The reason for such a good agreement is the appropriate selection of the temperature dependence of the inelastic collision number Z.

This parameter, which is in effect the inverse probability of the energy transfer between the internal modes of a dimer and the translational modes in dimer-monomer collisions, was found to be an important factor that influences the magnitude of the equilibrium constant K_{eq}. This may be explained as follows. The dimers are formed after three-body collisions, and typically have internal energies smaller than the evaporation energy after those collisions. In argon, the evaporation energy for a dimer is relatively small compared to the typical total collision energy for all temperatures under consideration ($E_{evap}/k \approx 140$ K). That means that most of the dimers will have their internal energy in excess of the evaporation energy just after one or two inelastic collisions with monomers for thermal bath temperatures greater than 140 K. The lifetime of the dimers whose internal energy is larger than the evaporation energy is very short, on the order of a picosecond. This results in the dimer-monomer energy transfer being the main process that leads to quick dimer dissociation. Note that the value of Z has negligible impact on the dimer formation rates, and only the evaporation rates are affected. As a result, in the range of temperatures considered in this work, the equilibrium constant for argon was found to be nearly proportional to Z^{-1}.

The Z dependence of the equilibrium constant is weaker for water condensation. In this case, the evaporation energy of a dimer is much larger than the translational energy of colliding molecules and dimers (the reduced evaporation energy $E_{evap}/k \approx 1,800$ K, compared to gas temperatures on the order of 300 K). The high value of the evaporation energy results in longer lifetimes of dimers, since many more collisions are necessary to transfer enough energy from the translational modes to the internal modes of a dimer. The dependence of K_{eq} on Z is therefore much weaker for water than for argon. In a 250 K thermal bath, K_{eq} was found to decrease by only about a factor of two when Z decreases from 10 to 1.

Comparison of the equilibrium constant obtained with the present model, with the theoretical results of Refs. 67, 74, where a flexible potential energy surface fitted to spectroscopical data was used, is shown in Fig. 3. Note that there are a number of theoretical predictions of the equilibrium rate of water dimerization, and they differ by at least a factor of three in the range of temperatures considered in this work. Reference[67] was chosen for comparison as the most sophisticated and one of the most recent ones. The results show that the calculated equilibrium constant agrees well with the theoretical prediction for temperatures between 160 K and 250 K, the range that is expected to be very important in terms of dimer formation and nucleation in plume expansions. The calculated values for higher temperatures significantly overpredict the theoretical curve. It is important to note that these results are sensitive to the values of C_v and E_{evap}. For example, a 20% change in C_v results in a factor of two difference in K_{eq}. However, the computations have shown that the change in the binding energy and heat capacity, that are assumed to be temperature independent, do not significantly change the slope of the equilibrium constant decreasing with increasing temperature. This general trend of weaker slope may be related to a number of factors, such as temperature dependence of actual heat capacity and evaporation energy, as well as the approximate after-reaction energy redistribution used in this work (recall that the Larsen-Borgnakke model was used for the energy redistribution). Another possible and likely reason is the temperature dependence of the dimer stabilization probability for three-body collisions, that was not included in the present model.

IV. ARGON CLUSTER SIZE DISTRIBUTION IN ORIFICE EXPANSION

The ability of a condensation model to reasonably capture theoretical dimer equilibrium constant and dimer formation rate at equilibrium is crucial for accurate prediction of the amount of dimers in a condensing gas flow. However, it does not guarantee correct rates for nucleation and evaporation of clusters larger than dimers. Therefore, in order to assess the model performance, it is necessary to compare cluster size distributions, obtained in numerical simulations, with available experimental data. Measurements of the pressure dependence

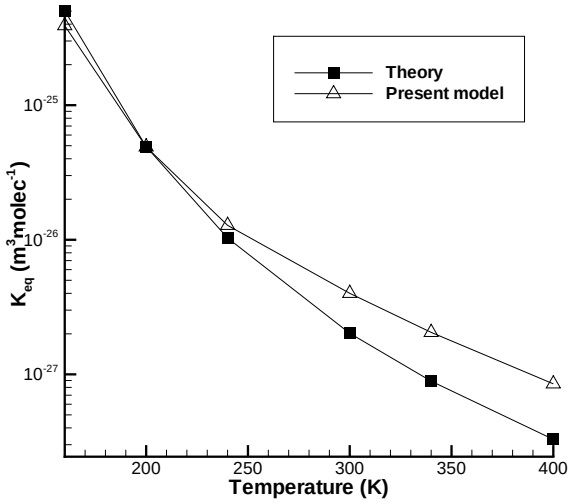

FIG. 3. Water equilibrium constant as a function of gas temperature.

of size selected argon clusters present a good validation tool for DSMC based condensation modeling. The reasons for selecting these measurements is that their operating Knudsen numbers, while rather low, are still high enough for the DSMC method to be used, and their accuracy is quite high. The results are based on the method of size selection of the clusters in a scattering process with He.[75,76] Originally designed to measure reliable fragmentation probabilities in the detection process, the data can also be used to measure the fractions of different cluster sizes as function of the pressure of the expansion.[76,77] The original data were complemented by new results up to $n = 10$ and newly evaluated using the recently obtained fragmentation probabilities in this size range.[78] The results for the averaged cluster sizes appeared already in Ref. 47.

In order to reproduce the experimental setup, an argon expansion out of a thin 40 μm diameter orifice was modeled, with a stagnation and orifice wall temperatures of 300 K. Two stagnation pressures were considered, 1.5 atm and 2 atm. The simulated part of the plenum was 70 μm in axial and radial directions, with the equilibrium stagnation conditions imposed at the inflow boundaries. The size of the subsonic part was chosen sufficiently large to minimize the impact of the orifice on the inflow boundaries. The plume part of the computational domain was stretched to 700 μm in the axial direction to capture the terminal argon cluster mole fractions, similar to those recorded in the experiments. Vacuum boundary conditions were imposed on the outflow boundaries. The the axis of symmetry boundary condition was imposed at the lower boundary. Fully diffuse accommodation on the wall was assumed. To avoid slow convergence associated with the subsonic part of the domain, the calculations included two steps. First, the flow was calculated in the free molecular regime. Then, the simulated molecules from the first step were utilized as the initial condition for the second, high pressure, step. The numbers of simulated molecules and collision cells were 8 million and 1.5 million, respectively.

The gas temperature field for the 1.5 atm stagnation pressure case is shown in Fig. 4 (left). Only part of the computational domain is shown to provide more detail to the plume near field. The gas density in the plenum is fairly high, which causes relatively large number of collisions in the plume. The latter results in low freezing temperatures, about 4 K along the nozzle axis. The flow starts to freeze after about 500 μm downstream from the orifice exit plane. The density of the expanding plume keeps its sharp decrease, as shown in Fig. 4 (right). The decreasing number of collisions in the flow, and especially three-body collisions that govern the dimer formation rate, results in freezing the mole fraction of argon clusters at 500 μm, which is also shown in Fig. 4 (right). Note that a smoothed mole fraction of all clusters is given in this figure. In the plenum, it is mostly dimers; their number in that region corresponds to the equilibrium mole fraction at a given temperature and density.

Comparison of computed and measured cluster size distributions for the two pressure under consideration is presented in Fig. 5. The relative mole fractions are given, with the combined total adding up to the unity. For the 1.5 atm case, there is a very good agreement between numerical modeling and experiment for dimers and trimer. For larger clusters, the computed values are lower than measured. Note that the statistical nature of the DSMC method makes it very difficult to calculate the concentration of cluster sizes which relative mole fraction is less than 0.01, with acceptable statistical accuracy. Even though each computation took days on a multi-processor computer, the values of the error bars for such cluster sizes are still on the order of the values of the corresponding mole fractions. The same is true for the experimental errors for the small fractions. Accounting for these numerical and experimental error bars, it may be concluded that there is a satisfactory agreement between the modeling and the measurement for the 1.5 atm case. For 2 atm, the mole fractions of the clusters larger than trimers are noticeably higher than for 1.5 atm, and the agreement between the DSMC and the experiment is better. Again, the computational and experimental points agree within the limits of uncertainties of the used techniques and models. Note also that the computed dimer mole fraction is in reasonable agreement with the Knuth's semiempiric expressions[46]. Knuth's non-dimensional scaling parameter, that defines the dimer mole fraction, is 0.0037 and 0.006 as compared to the DSMC values of 0.0053 and 0.009 for pressures of 1.5 atm and 2 atm, respectively.

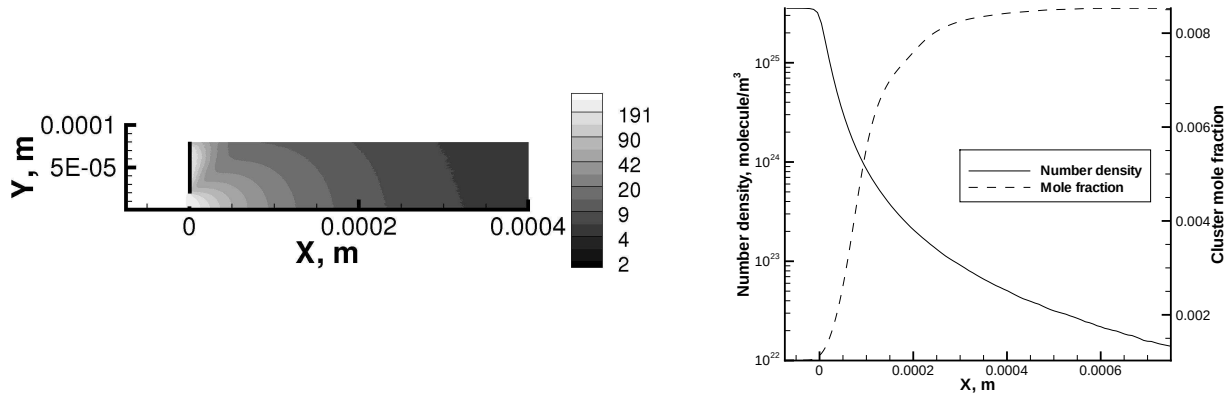

FIG. 4. Gas temperature field (left) and number density and cluster mole fraction profiles along the orifice axis (right) in argon orifice expansion. 1.5 atm case.

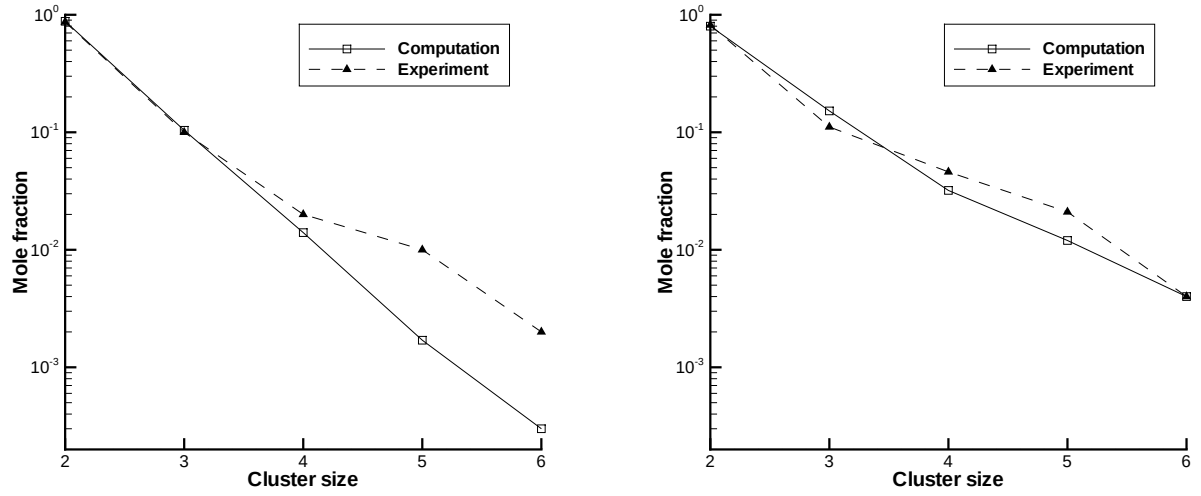

FIG. 5. Terminal argon cluster relative mole fraction for a stagnation pressure of 1.5 atm (left) and 2.0 atm (right).

V. WATER CLUSTER SIZE DISTRIBUTION IN NOZZLE FLOW

The last part of the validation and numerical analysis of the presented condensation model is focused on the nucleation and evolution of small water clusters in a conical nozzle. The study was prompted by the availability of high quality experimental data[48] on terminal size distribution of water clusters in the range of flow conditions where the pressure was relatively low so that the computational cost of using the DSMC method is not prohibitive (although still rather high). The results are obtained by doping the water clusters by one Na atom, which is photoionized close to the threshold without fragmentation. The results are presented for the nozzle geometry of Ref. 48. The nozzle is a conical nozzle with a 41° opening angle, a total length of 2 mm, and a throat diameter of 50 μm. The two smallest stagnation pressures considered in Ref. 48, 1.577 bar and 2.173 bar, are used in this work, with the corresponding stagnation temperature of 495 K. A constant nozzle wall temperature of 495 K was used to reproduce the experimental setup. Since the background pressure effect in the experiment is believed to be small,[79] the flow expansion into the vacuum is modeled.

The axisymmetric capability of SMILE was used, with the total number of simulated molecules and collision cells about 80 million and 10 million, respectively, for a pressure of 1.577 bar, and 160 million and 20 million for a pressure of 2.173 bar. A uniform 400×100 grid was used for sampling of macroparameters and distribution functions. The Larsen-Borgnakke model with constant

relaxation numbers of 10 for both rotational and vibrational energies was used for energy transfer in monomer-monomer collisions, and the reflection of particles on the nozzle surface was assumed to be fully diffuse. Uniform inflow conditions were imposed at the nozzle throat, calculated from the isentropic flow relations.

The first set of results presented here shows the effect of the condensation on the gas flow inside the nozzle and in the plume near field. The gas translational temperature and axial velocity is shown in Fig. 6 for two cases, the baseline condensation model and the condensation turned off. The results show that the condensation practically does not change the flow parameters inside the boundary layer. This is expected, since the temperature in the boundary layer is higher than in the coreflow, and nucleation near the surface is not likely. Near the centerline, though, the condensation, being an exothermic process, results in a significant heat release. The temperature in that region visibly increases, with the maximum change of over 20 K. The higher temperature for the condensing flow, accompanied by fast translational relaxation, causes an increase in the axial velocity in the coreflow of about 30 m/s. The velocity change inside the boundary layer is negligibly small.

The computations conducted for a higher stagnation pressure of 2.173 bar show visible effects of pressure on both gas temperature and number of clusters in the flow (see Fig. 7). As expected, the boundary layer thickness decreases with increasing pressure. The temperatures in the coreflow are similar only during the first 100 μm from the nozzle throat. Further downstream, mostly due to the condensation heat release, the temperature in the coreflow is up to 15 K higher for the larger pressure case. The cluster mole fraction is also noticeably higher. Generally, the cluster concentration increases rapidly in the first 100μm from the nozzle throat, and reaches its maximum at about 300μm for the 1.577 bar case and 200μm for 2.173 bar. After that, the evaporation and cluster coalescence result in some decrease of the cluster concentration. The maximum mole fraction is 1.5% for the lower pressure case, and 2.5% for the higher pressure case. In addition to an increase in the number of clusters with stagnation pressure, the average cluster size also slightly increases with pressure, although this increase is much less pronounced that that of the total number of clusters. The average terminal cluster size is about 4.1 and 4.2 for 1.577 bar and 2.173 bar, respectively.

Comparison of the terminal size distribution obtained using the presented model, with experimental results[48] is shown in Fig. 8. In the experiments, the dimers were below the detection threshold, the trimer population may be somewhat affected by that threshold, and all larger clusters are believed to be recorded without significant distortions. Exponential profiles of the size distribution function, $f \propto \exp\left(-\frac{n}{\langle n\rangle}\right)$, that have the average cluster size $\langle n\rangle$ that corresponds to the experimental values of 7 and 20, are also shown in this figure. For side-by-side comparison, the experimental size distribution was normalized so that it has the same fraction of clusters larger than dimers as in the exponential distribution approximating it.

The results show that there is a reasonable agreement between the numerical modeling and measurements for the lower pressure. The computed average cluster size for 1.577 bar was 5.5, as compared to the measured value of 7$\pm$2. This value is based on a reevaluation of the data by correctly subtracting the background. There is a local maximum for the cluster size of 8 observed in the computations, whereas in the experiment it is observed at $n = 6$. The reason for such a local maximum is believed to be the relation between the evaporation energies and heat capacities for the corresponding cluster sizes (see Table III). It is clear that the values of these parameters, used in the numerical modeling, need further refinement, and accurate theoretical data for them are indispensable for obtaining better agreement with the data. The agreement between numerical and experimental results deteriorates with pressure, which is primarily related to inaccurate values of the evaporation energies and heat capacities of larger clusters. Note that no accurate quantum mechanical values for these properties were found in the literature for clusters larger than 10-mers, and the availability of this information is critical for the present model (and any other kinetic model of condensation). The rough agreement of the data with an exponential profile indicates that the cluster formation is mainly based on monomer addition.

VI. CONCLUSIONS

A non-equilibrium condensation model applicable for the DSMC method is constructed. An important and distinguishing aspect of the present model is that all condensation-related processes are defined at the microscopic level, and all collision, nucleation, and evaporation events depend on instantaneous energies of colliding partners, and not cell temperature or other macroscopic quantities. The model was validated through comparison with available theoretical and experimental data on condensation rates in a thermal bath, dimer mole fractions in orifice expansions, and cluster size distributions in nozzle flows. The model is based on a DSMC model of recombination reaction for the collision based dimer formation, and the RRK model for the cluster evaporation. Cluster growth is modeled through cluster-monomer and cluster-cluster collisions. The energy transfer in these collisions is calculated using the extended Larsen-Borgnakke principle. The nucleation rate was found highly sensitive to the values of heat capacity of clusters.

Two gases are considered in this work, argon and water. For the thermal bath relaxation, the present model was found to capture the dimer equilibrium constants for water and argon and dimer nucleation rates for argon fairly well in the considered range of temperatures from 100 K to 350 K. The computed slope was somewhat

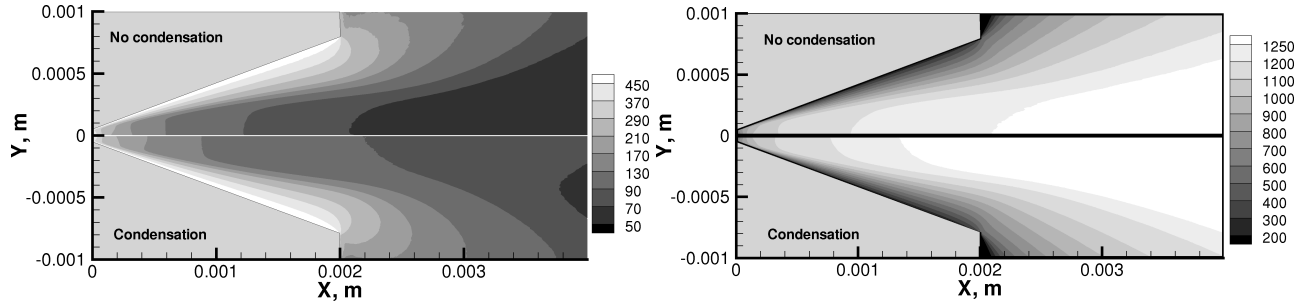

FIG. 6. Impact of the condensation on the water translational temperature (K), left, and axial velocity (m/s), right.

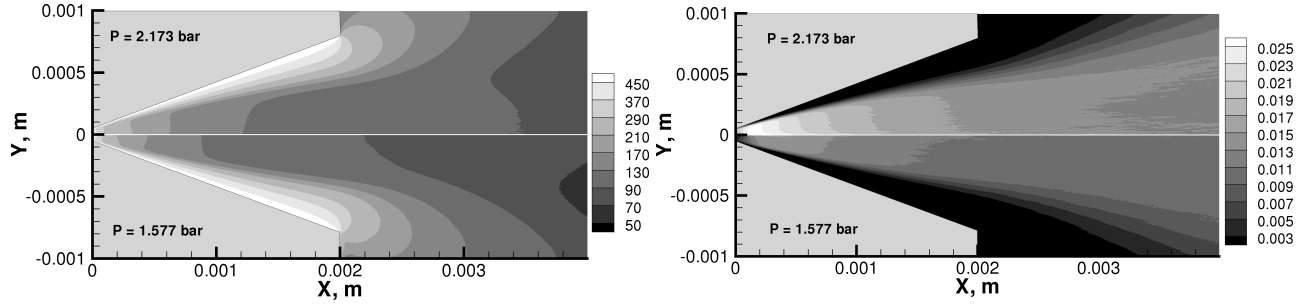

FIG. 7. Impact of the stagnation pressure on the water translational temperature (K), left, and cluster mole fraction, right.

smaller than theoretical for water clusters, which may be attributed to the accuracy of used physical and numerical parameters of the condensation model.

Comparison of terminal mole fractions in a sonic orifice expansion of argon with available experimental data showed that the new model agrees reasonably with the measurements. For water, agreement is reasonable only for stagnation pressures of about 1.5 bar, while for higher pressures the present model underpredicts the population of clusters larger than 10-mers. More accurate values for the heat capacity and evaporation energy of such clusters are needed to obtain better agreement with the data.

VII. ACKNOWLEDGMENTS

The authors are extremely thankful to Dr. Matthew Braunstein for his help with water binding energy analysis, and Dr. Y. Scribano for providing additional data for water dimer equilibrium constant and heat capacity. The work was supported by the Air Force Office of Scientific Research.

[1] S.L. Girshick, P. Agarwal, and D.G. Truhlar, J. Chem. Phys. **131**, 134305 (2009).
[2] S.R.T. Cromie and P. Ballone, J. Chem. Phys. **131**, 034906 (2009).
[3] D. Brus, V. Zdimal, and H. Uchtmann, J. Chem. Phys. **131**, 074507 (2009).
[4] S.M. Kathmann, G.K. Schenter, and B.C. Garrett, J. Chem. Phys. **131**, 5046 (2002).
[5] F. Abraham, *Homogeneous Nucleation Theory: The Pretransition Theory of Vapor Condensation* (Academic Press, New York, 1974).
[6] A. Telemeter, *Nucleation Phenomena* (Wiley, New York, 1977).
[7] A. Itkin and E. Kolesnichenko, *Microscopic Theory of Condensation in Gases and Plasma* (World Scientific, Singapore, 1997).
[8] P. ten Wolde and D. Frenkel, J. Chem. Phys. **109**, 9901 (1998).
[9] H. Hettema and J. McFeaters, J. Chem. Phys. **105**, 2816 (1996).
[10] S. Girshick, J. Chem. Phys. **94**, 826 (1991).
[11] J. E. McDonald, Am. J. Phys. **31**, 31 (1963).
[12] B. S. Lukyanchuk, W. Marine, S. I. Anisimov, and G. A. Simakina, *Proceedings of SPIE* **3**(618), 434 (1999).
[13] H. Haberland, in *Clusters of Atoms and Molecules* (Springer, Berlin, 1994).
[14] M. A. Ratner, Low Temp. Phys. **25**, 266, (1999).
[15] Yu. P. Raizer, Soviet Physics JETP **37**, 1229, (1959).
[16] J. Zhong, M. Zeifman, S. Gimelshein, and D. Levin, AIAA Journal **43**(8), 1784 (2005).
[17] J. Zhong, D. A. Levin, and M. I. Zeifman, Proc. XXIV Int. Symp. on Rarefied Gas Dynamics, *AIP Conference Proceedings* **762**, 391 (2005).
[18] W. Williams and J. Lewis, *Summary report for the CONSET program at AEDC* (Arnold Engineering Development Center, AEDC-TR-80-16, 1980).
[19] M. Ohkubo, B. Kuwata, B. Lukyanchuk, and T. Yabe, Appl. Phys. A **77**, 271 (2003).
[20] M. Sharaf and R. Dobbins, J. Chem. Phys. **77**, 1517, (1982).
[21] M.I. Zeifman, J. Zhong, and D.A. Levin, Proc. XXIV Int. Symp. on Rarefied Gas Dynamics, *AIP Conference Proceedings* **762**, 509 (2005).
[22] D. Willis, B. Hamel, and J. Lin, Phys. Fluids **15**, 573 (1972).
[23] R. Cattolica, F. Robben, L. Talbot, and D. Willis, Phys. Fluids **17**, 1793, (1974).
[24] G. Bird, Phys. Fluids **19**, 1486 (1976).
[25] G. Schenter, S. Kathmann, and B. Garrett, J. Chem. Phys. **110**, 7951, (1999).
[26] G. K. Schenter, S. M. Kathmann, and B. C. Garrett, Phys. Rev. Lett. **82**, 3484, (1999).
[27] B. Senger, P. Schaaf, D. S. Corti, R. Bowles, J. C. Voegel, and H. Reiss, J. Chem. Phys. **110**, 6421, 1999.
[28] B. Senger, P. Schaaf, D. S. Corti, R. Bowles, D. Pointu, J. C. Voegel, and H. Reiss, J. Chem. Phys. **110**, 6438, (1999).

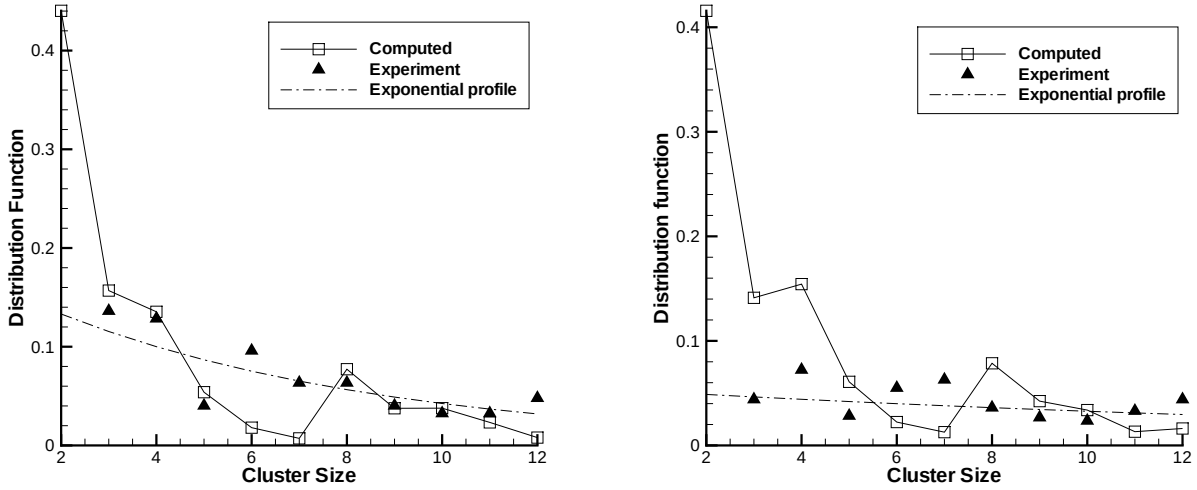

FIG. 8. Comparison of the computed size distribution with experimental data of Ref. 48 for 1.577 bar (left) and 2.173 bar (right).

[29] J. Soler, N. Garcia, O. Echt, K. Sattler, and E. Recknagel, Phys. Rev. Lett. **49**, 1857 (1982).

[30] M. Valerica, M. Casey, J. Goodisman, and J. Chaiken, J. Chem. Phys. **98**, 4610 (1993).

[31] S. Toxvaerd, J. Chem. Phys. **115**, 8913 (2001).

[32] T. Ikeshoji, B. Hafskjold, Y. Hashi, and Y. Kawazoe, J. Chem. Phys. **105**, 5126 (1996).

[33] M. I. Zeifman, J. Zhong, D. A. Levin, *AIAA Paper 2004-2586* (2004).

[34] M. Zeifman, B. J. Garrison, and L. V. Zhigilei, J. Appl. Phys. **92**, 2181 (2002).

[35] G. A. Bird, *Molecular Gas Dynamics and the Direct Simulation of Gas Flows* (Clarendon Press, Oxford, 1994).

[36] H. Mizuseki, Y. Jin, Y. Kawazoe, and L. T. Wille, J. Appl. Phys. **87**, 6561 (2000).

[37] H. Mizuseki, K. Hongo, Y. Kawazoe, and L. Wille, Comp. Mat. Sci. **24**, 88 (2002).

[38] J. Zhong, M. Zeifman, and D. Levin, J. Thermophysics and Heat Transfer **20**(1), 41 (2006).

[39] A. Gallagher-Rogers, J. Zhong, and D. A. Levin, *AIAA Paper 2007-4159* (2007).

[40] J. Zhong and D. Levin, AIAA Journal **45**(4), 902 (2007).

[41] B. Briehl and H. Urbassek, J. Vac. Sci. Tech. A **17**(1), 256 (1999).

[42] S. Gratiy, J. Zhong, D. A. Levin, *AIAA Paper 2006-3598*, (2006).

[43] M. F. Jarrold, in *Clusters of Atoms and Molecules* (Springer, Berlin, 1994).

[44] R.D. Levine, *Molecular reaction dynamics* (Cambridge University Press, Cambridge, 2005).

[45] S. F. Gimelshein and M. S. Ivanov, *Proc. XVII Int. Symp. on Rarefied Gas Dynamics,* AIAA Series *Progress in Astronautics and Aeronautics* Vol. 159, 218 (AIAA, Washington DC, 1994).

[46] E. L. Knuth, J. Chem. Phys. **101**(21) 9125 (1997).

[47] U. Buck and R. Krohne, "Cluster size determination from diffractive He atom scattering", J. Chem. Phys. **105**, 1996, 5408-5415.

[48] C. Bobbert, S. Schutte, C. Steinbach, U. Buck, "Fragmentation and reliable size distributions of large ammonia and water clusters," Eur. Phys. J. D **19** pp. 183-192, 2002.

[49] D. L. Bunker, J. Chem. Phys. **32**(4), 1001 (1959).

[50] M. S. Ivanov and S. V. Rogasinsky, Sov. J. Numer. Anal. Math. Modelling **2**(6), 453 (1988).

[51] G. A. Bird, *Proc. XI Int. Symp. on Rarefied Gas Dynamics,* AIAA Series *Progress in Astronautics and Aeronautics* Vol. 74, 239 (AIAA, Washington DC, 1981).

[52] C. Borgnakke and P. S. Larsen, J. Comp. Phys. **18**, 405 (1975).

[53] J. Zhong, M. I. Zeifman, and D. A. Levin, J. Thermophysics and Heat Transfer **20**(3), 517 (2006).

[54] P. F. Zittel, D. E. Masturzo, J. Chem. Phys. **90** 2), 977 (1989).

[55] N. E. Gimelshein, *Enhanced direct simulation Monte Carlo models for internal energy exchange and chemical reactions,* M.S. Thesis, Penn State (2002).

[56] J. F. Crifo, ICARUS, **84**, 414 (1990).

[57] Z. Li, J. Zhong, D. A. Levin, and B. J.Garrison, AIAA Journal **47**(5), 1241 (2009).

[58] Y. Okada and Y. Hara, Earozoru Kenkyu **22**(2), 147 (2007).

[59] J. Zhong, N. Moghe, Zh. Li, and D. A. Levin, Phys. Fluids **21**, 036101 (2009).

[60] M. Braunstein, Private communication, 2009.

[61] S. S. Xantheas, C. J. Burnham, R. J. Harrison, J. Chem. Phys. **116**, 1493 (2002).

[62] K. Diri, E. M. Myshakin, and K. D. Jordan, J. Phys. Chem. **109**, 4005 (2005).

[63] H. M. Lee, S. B. Suh, J. Y. Lee, P. Tarakeshwar, and K. S. Kim, J. Chem. Phys. **112**, 9759 (2000).

[64] J. T. Su, X. Xu, and W. A. Goddard III, J. Phys. Chem. A **108**, 10518 (2004).

[65] L. L. Lohr, Molecular Physics **85**(3), 607 (1995).

[66] P. A. Frantsuzov and V. A. Mandelshtam, J. Chem. Phys. **128**, 094304 (2008).

[67] Y. Scribano, N. Goldman, R. J. Saykally, and C. Leforestier, J. Phys. Chem. A **110**(16), 5411 (2006).

[68] S. A. Losev, S. O. Macheret, B. V. Potapkin, and G. G. Chernyi, *Physical and chemical processes and gas dynamics: cross sections and rate constants* AIAA Series *Progress in Astronautics and Aeronautics*, Vol. 196 (AIAA, Washingtoin DC, 2002).

[69] M. S. Ivanov, G. N. Markelov, and S. F. Gimelshein, Computers and Mathematics with Applications **35**(1-2), 113 (1998).

[70] R. Kalus, J. Chem. Physics **109**(19), 8289 (1998).

[71] P. S. Dardi and J. S. Dahler, J. Chem. Phys. **93**(5), 3562 (1990).

[72] R. E. Leckenby and E. J. Robbins, Proc. Royal Soc. London A, 389 (1966).

[73] D. E. Stogryn and J. O. Hirschfelder, J. Chem. Phys. **31**(6), 1531 (1959).

[74] Y. Scribano, Private Communication, 2009.

[75] U. Buck and H. Meyer, J. Chem. Phys. **84**, 4854 (1986).

[76] U. Buck, J. Phys. Chem. **92**, 1023 (1988).
[77] U. Buck and H. Meyer, Surf. Sci. **156**, 275 (1985).
[78] P. Lohbrandt, R. Galonska, H. J. Kim, M. Schmidt, C. Lauenstein, and U. Buck, in *Atomic and Molecular Beams. The State of the Art 2000*, edited by R. Campargue (Springer, Berlin, 2001), p. 623.
[79] S. Schütte and U. Buck, Int. J. Mass Spec. **220**, 183 (2002).